Tracking at LHC

F. Ragusa[1] and L. Rolandi[2]

[1]Dipartimento di Fisica, Università di Milano and INFN, Sezione di Milano, via Celoria 16, I-20133 Milano, Italy
[2]CERN, PH Department, CH-1211 Genéve 23, Switzerland

E-mail: francesco.ragusa@mi.infn.it gigi.rolandi@cern.ch

Abstract. Precise tracking is an indispensable tool for the study of many phenomena at new energy frontier accessible with the CERN Large Hadron Collider. The tracking detectors of ATLAS and CMS have been designed to cope with the harsh experimental conditions of the LHC interaction region. In this paper we discuss and compare the tracking performance of these two detectors.

PACS numbers: 07.05.Fb, 29.30.Aj, 29.40.Gx, 29.40.Wk

Submitted to: *New J. Phys.*

1. Introduction

The first motivation for experimentation at the TeV scale is the study of the Electroweak Symmetry breaking. In the framework of the Standard Model the breaking of the symmetry is induced by the Higgs mechanism. However it is possible that the experimentation at the TeV scale will reveal new phenomena: the known existence of the Dark Matter in the Universe and the fact the Standard Model Higgs mass is unstable to radiative corrections strongly indicate that the experimentation in the TeV region will lead to the discovery of new constituents or new symmetries of matter or new forces.

Precise tracking is an indispensable tool for any collider experiment. Efficient identification of electrons and muons, based on tracking, is necessary to separate new phenomena from the overwhelming QCD background. Lepton signatures require muon tracking-based trigger and precise measurement of the momentum of muons and electrons. Additional neutral gauge bosons (Z') predicted in many new physics scenarios [1] can be identified through their decay into muons and electrons in events selected by muon or electron based triggers. The forward-backward asymmetry of leptons in the decay of the Z' is measured from the curvature of the lepton tracks in the magnetic field of the detector. It gives information on parity violating couplings and helps in distinguishing among different theoretical models. At LHC Z and W

bosons are identified through their leptonic decays and used both to discover new physics phenomena and to calibrate the detectors.

The capability to reconstruct detached vertices to identify long-lived particles is an essential tool for the precise study of the top quark, the heaviest and least studied of the six known quarks. Tagging b-jets is also an essential tool in discovery physics in all cases when the new particles have a preferential decay to heavy quarks, like the Higgs Bosons of the Supersymmetry.

Cross sections of new and known interesting phenomena at TeV scale are typically small: between 1 pb and 1 nb . The study of these processes requires colliders with large luminosities which are achieved using high bunch-crossing frequency. This poses severe constraints on the response time of the tracking devices. At LHC the cross sections for low p_{t} phenomena are large, typically 100 mb, and many low p_{t} events are produced at each bunch crossing. Their tracks are superimposed to those produced in the rare high p_{t} collisions leading to very complex patterns that can be reconstructed efficiently only by high granularity devices with good time resolution.

At the TeV scale the pattern recognition has the additional challenge of precisely reconstructing the tracks of narrow jets produced by highly boosted low mass particles like high energetic b-jets. The most challenging task is the efficient reconstruction of the three tracks originating from the decay of a very energetic tau lepton.

This paper describes and compares the tracking performance of the two general purpose detectors at LHC: ATLAS [2] and CMS [3]. Both detectors are now in the final installation phase. Their performance is presently being re-evaluated by the Collaborations while the figures given in this paper reflect the published expected performance. Many of the plots shown here have been redrawn using the information of the published plots in order to present the figures on the same scale for an easy comparison.

2. Charged particles tracking in magnetic field

The trajectory of a charged particle of momentum p and (signed) charge q in a static magnetic field $\boldsymbol{B}(\boldsymbol{r})$ is given by the differential equation

$$\frac{\mathrm{d}^2\boldsymbol{r}}{\mathrm{d}s^2} = \frac{q}{p}\frac{\mathrm{d}\boldsymbol{r}}{\mathrm{d}s} \times \boldsymbol{B}(\boldsymbol{r}) \tag{2.1}$$

where $\mathrm{d}s = v\mathrm{d}t$ is the distance along the trajectory. The vector $\mathrm{d}^2\boldsymbol{r}/\mathrm{d}s^2$ is perpendicular to the trajectory and its length is $1/R$, where $R(s)$ is the curvature radius of the trajectory; the vector $\mathrm{d}\boldsymbol{r}/\mathrm{d}s$ is tangent to trajectory and has unit length. The integral

$$\int \mathrm{d}\alpha = \int \frac{\mathrm{d}s}{R} = \int \left|\frac{\mathrm{d}^2\boldsymbol{r}}{\mathrm{d}s^2}\right| \mathrm{d}s = \frac{q}{p}\int \left|\frac{\mathrm{d}\boldsymbol{r}}{\mathrm{d}s} \times \boldsymbol{B}(\boldsymbol{r})\right| \mathrm{d}s \tag{2.2}$$

provides the bending angle of a charged particle after passing through a magnetic field. The integral on the right side of 2.2 is referred to as *bending power* and is the integral

along the trajectory of the normal component of $\boldsymbol{B}$. The transverse displacement δ of a particle after a path length ℓ perpendicular to the magnetic field is $\delta = \ell\alpha/2$, if $\ell << R$.

In high-energy experiments the coordinates along the trajectory are measured with position sensitive detectors. The data from the detectors are analyzed by a pattern recognition program that associates coordinate measurements to trajectories (*tracks*). Equation 2.1 is used together with the magnetic field map to fit the measurements to a model of the track. The most important parameters of the track are its momentum vector and point of origin. The reconstructed tracks are then combined to find the primary and secondary (detached) vertices in the event.

The most popular approach to track finding and fitting is the combinatorial Kalman filter [4] where the full knowledge of the track parameters at each detector layer is used to find compatible measurements in the next detector layer, forming combinatorial trees of track candidates. Generalizations of the Kalman filter are the Gaussian Sum filter [5], which is used to account for the bremsstrahlung energy loss of electrons, and the Adaptative methods [6], which are used for vertex reconstruction.

In this paper we will not address the problem of the optimal track fit, for which many excellent articles exist (see for example [7]). Instead we intend to review the tracking detectors of ATLAS and CMS and to discuss the ideas behind the designs and how they affect physics performance. For this purpose we introduce a simplified formulation of the tracking problem outlined above by assuming a helicoidal trajectory in an uniform magnetic field.

At large momentum the trajectory can be approximated with a straight line $y = a+bz$ in the plane containing the magnetic field and with a parabola $y = a+bx+(c/2)x^2$ in the bending plane perpendicular to the magnetic field. The parameter of the quadratic term is related to the the momentum of the particle in the bending plane $p_{\rm t}$ through the radius of the circumference $c = -R^{-1}$. We now consider the track fit in the two planes and discuss the error on the impact parameter and on the particle momentum and how they are related to the design of a spectrometer.

Straight line fit. Let us consider $N + 1$ position sensitive detectors having a measurement error σ, equally spaced and placed at positions $z_0, \ldots, z_N$ [8]; the spectrometer length is $L = z_N - z_0$ and the distance of its center from the interaction point is $z_{\rm c} = (z_0 + z_N)/2$.

Choosing a reference frame with the origin at the center of the track, the errors on the track parameters a and b are are uncorrelated ($\sigma_{\rm ab} = 0$), and the error on the extrapolation at the interaction point is given by

$$\sigma^2_{\rm ip} = \sigma^2_{\rm a} + \sigma^2_{\rm b} z^2_{\rm c} = \frac{\sigma^2}{N+1} + \frac{\sigma^2}{N+1}\frac{12N}{N+2}\frac{z^2_{\rm c}}{L^2}. \tag{2.3}$$

The above formula shows how the error of the impact parameter depends on the error of the slope of the track (σ_b) and on the distance of the center of the spectrometer from the interaction point (z_c). To minimize the error on the impact parameter we have to:

- use detectors with excellent spatial resolution σ;

- make the spectrometer as long as possible to reduce the error on the slope;
- place the spectrometer as close as possible to the interaction point.

Excellent spatial resolution is obtained with silicon detectors designed to have $\sigma \sim 10$ μm or better. As such detectors are very expensive, the maximum spectrometer length L is limited. To overcome this limitation, the spectrometers are usually split into an inner vertex detector and a central tracking detector. The latter can be made long (large L) making the error on the slope small. Compact pixel vertex detectors provide excellent spatial resolution very near to the interaction point.

The quadratic fit and the measurement of the momentum. Let us consider $N+1$ measuring detectors equally spaced and placed at positions $x_0, \ldots, x_N$ [9]. The spectrometer length is $L = x_N - x_0$. The error on the coefficient of the quadratic term is

$$\sigma_{\rm c}^2 = \frac{\sigma^2}{L^4} A_N \qquad\qquad A_N = \frac{720N^3}{(N-1)(N+1)(N+2)(N+3)}$$

Since $c = -R^{-1}$ the error on the transverse momentum $p_{\rm t}$ is given by

$$\frac{\delta p_{\rm t}}{p_{\rm t}} = \frac{p_{\rm t}}{q}\frac{\sigma}{BL^2}\sqrt{A_N} = \frac{p_{\rm t}c}{qc}\frac{\sigma}{BL^2}\sqrt{A_N} = p\frac{\sigma}{0.3BL^2}\sqrt{A_N} \tag{2.4}$$

where we have used the common units GeV, Tesla and meter. The formula illustrates the basic features of the momentum measurement with a magnetic spectrometer:

- the relative transverse momentum resolution is proportional to the transverse momentum;
- the strong dependence on the spectrometer length L calls for large detectors to achieve good momentum resolution;
- the transverse momentum resolution is inversely proportional to the magnetic field;
- the dependence on the number of measured coordinates is weak; however the number of coordinates is important for the robustness of the pattern recognition.

An alternative formulation introduces the *sagitta* h of the track that is the maximum excursion of a circular segment over the corresponding chord. For $L << R$, we can approximate

$$h = \frac{L^2}{8R} = \frac{0.3BL^2}{8p_{\rm t}}. \tag{2.5}$$

The extrapolation in the magnetic field affects also the uncertainty of the impact parameter. Compared to the simple case discussed in equation (2.3) the general formula contains additional terms that may further degrade the precision and that account for the error in the extrapolation back to the origin caused by the uncertainty on the curvature of the track [8].

Multiple scattering. The uncertainty of the track parameters is affected by multiple scattering [8, 9] of the charged particle by the material of the spectrometer. A particle of momentum p and unit charge traversing a path length x of material, characterized

by a radiation length X_0, is deflected by multiple Coulomb scattering from nuclei. The projection of this deflection angle on any plane containing the original direction is roughly gaussian distributed around zero with a root mean square width given by [10]

$$\theta_{\rm rms} = \frac{13.6MeV}{\beta p}\sqrt{\frac{x}{X_0}} \tag{2.6}$$

The random deflection smears the position measurements and introduces a correlation among position measurements downstream of the material causing the deflection. Assuming that the position accuracy is dominated by multiple scattering, the momentum resolution for a spectrometer of length L and $N+1$ equally spaced position measurements is given by [8, 9]

$$\frac{\delta p_{\rm t}}{p_{\rm t}} = \frac{1}{0.3B}\frac{0.0136}{\beta}\sqrt{\frac{C_N}{X_0 L}} \tag{2.7}$$

C_N is an N-dependent coefficient [9] which is equal to 1.3 within 10% accuracy. When multiple scattering dominates, the relative momentum resolution does not depend on the momentum and has a weak dependence on the length of the spectrometer.

At colliders, secondary vertices of short lived particles are contained within the beam pipe. For particles of low momentum the multiple scattering in the material of the beam pipe becomes a significant source of error. A track measured with infinite precision outside the beam pipe when extrapolated to the origin misses the primary vertex by a randomly distributed distance d which has roughly gaussian distribution with a width $d_{\rm rms} = R_{\rm bp}\theta_{\rm bp}$, where $R_{\rm bp}$ is the radius of the beam pipe and $\theta_{\rm bp}$ the rms multiple scattering angle due to the beam pipe material.

3. The LHC *pp* collider

The main design parameters of the LHC machine are the proton beam energy of 7 TeV and the peak luminosity of 10^{34} cm^{-2} sec^{-1}. This luminosity is achieved by crossing very dense bunches containing about 10^{11} protons every 25 ns. Multiple inelastic collisions, called *pile-up* events, occur at each bunch crossing with an average of about 20 collisions per crossing. Each inelastic collision produces on average 4 charged particles per unit rapidity resulting in some 400 charged particles traversing the sensitive volume of the central tracker every 25 ns.

The average transverse momentum of these pile-up particles is 0.7 GeV, more than half of which cross the entire tracking volume and to reach the electromagnetic calorimeter without curling in the magnetic field. Given the very small bunch crossing period, most of the particles produced during one bunch crossing are still inside the detector when the next collisions occur: in 25 ns a high $p_{\rm t}$ particle goes some 7 meters away from the interaction point, while a low $p_{\rm t}$ particle may curl 2-3 times inside the tracker.

The particles of the rare high $p_{\rm t}$ collisions of interest are produced together with the pile-up particles of the same bunch crossing. They traverse the detector simultaneously

and the pattern recognition algorithm must be able to reconstruct all these tracks in the same event. Once the tracks from pile-up events are reconstructed they can be identified and discarded because they come from a different primary vertex. Since the luminous area of LHC has a gaussian sigma along the beam direction of ~ 8 cm, the vertices of the different inelastic collisions are separated by about 1 cm on average.

The complexity of the pattern recognition increases as a function of the occupancy, which is defined as the average number of hits per event in one elementary detector element. In low occupancy environments the probability that two tracks overlap in the same elementary detector is small and the number of ambiguities is small. High pattern recognition efficiency is obtained with occupancies smaller than 1%. The track density per bunch crossing of the pile-up events on a detector layer at a radius r and at $\eta = 0$ is about $40 \times 1/r^2$. In order to obtain occupancy smaller than 1%, the elementary detector element must cover a surface that is smaller than $0.00025 \times r^2$. This figure is equivalent to the surface covered by a 10 cm long strip of a 100 μm pitch silicon detector placed at 20 cm from the beam line. Deviations up to a factor ~ 3 from this simple model are caused by the magnetic field which curls low momentum particles at small radii.

The flux of particles irradiates the tracking detectors and causes radiation damage. Additional radiation originates from interactions with the detector material like photon conversions and nuclear interactions. Due to interactions in the calorimeters, the trackers are penetrated by significant neutron radiation at large radii.

ATLAS and CMS both use silicon detectors for the innermost part of their tracking systems. The main radiation damage to silicon comes from bulk defects due to the displacements of the lattice atoms and the subsequent annealing dynamics. The observed deterioration depends on the fluence, on the type and energy of the radiation. The radiation fluences are usually normalized comparing to the damage caused by 1 MeV neutrons ($n_{\rm eq}$). For a peak luminosity of 10^{34} cm^{-2} sec^{-1} the expected annual fluence (in units of $10^{13} n_{\rm eq}$ cm^{-2}) varies from 26 in the innermost tracking layer (~ 4 cm radius) to about 0.6 at a radius of 50 cm [11].

The presence of pile-up tracks and the high radiation environment pose severe constraints on the design of the central trackers, which cover the region up to $r \sim 1$ m:

- the response times of the detector elements and their read-out electronics has to be fast enough to process the event in less than 25 ns to minimize the pile-up to only one bunch crossing;
- the granularity of detector elements must be very high to keep the occupancy low;
- all elements of the detector, including active material, read-out electronics and cables must be resistant to the high radiation.

These constraints are significantly relaxed for the muon chambers which are installed at $r > 4$ m and are shielded by the calorimeters. Here the pile-up tracks are not an issue and the constraint on the response time is relaxed. While these detectors integrates many bunch crossing, they must be capable to to identify the bunch crossing of each particle that they track.

4. The tracking systems of ATLAS and CMS

The layouts of ATLAS and CMS are shown in figure 1. The most notable difference between the two detectors is the total volume, which is determined by the strategy to measure muon momenta. ATLAS has chosen a stand-alone system based on three superconducting toroid magnets and a set of very large and precise chambers the alignment of which is constantly monitored with optical devices [12]. CMS identifies and tracks muons in the iron of the yoke of a 4 Tesla, large bore magnet providing a coarse measurement of the sagitta, which is eventually refined by the association to the track measurement in the inner detector [13].

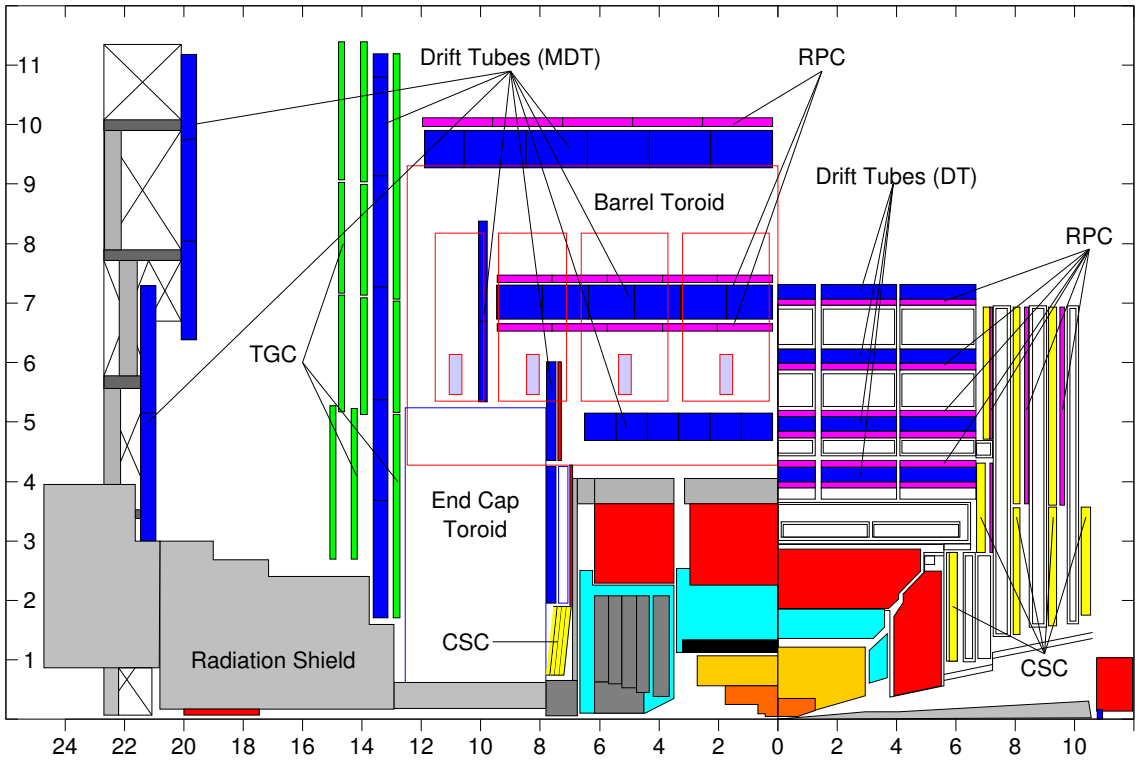

Figure 1. Side view of one quadrant of the ATLAS [12] (left) and of the CMS [3] (right) muon spectrometers. Note the difference of a factor ~ 2 between the horizontal and vertical scales.

4.1. The muon tracking systems

In the ATLAS barrel the magnetic field is produced by a toroidal magnet extending over a length of 25 m, with a bore of 9.4 m and an outer diameter of 20.1 m. The two end-cap toroids have a length of 5 m with a bore of 1.65 m and an outer diameter of 10.7 m. Each toroid consists of 8 superconducting coils symmetrically positioned around the beam axis; the coils of the two end-caps are rotated by 22.5° with respect to the barrel toroid to optimize the bending power in the transition region between the barrel and the end-cap magnets. The magnets provide an average magnetic field of 0.5 T with peak

value up to approximately 2.6 T in the barrel and 4 T in the end-caps; typical bending powers are 3 Tm in the barrel and 6 Tm in the end-caps.

The CMS 4 T magnetic field is produced by a 13 meters long solenoid with a bore of 6 meters. The bending power inside the coil is 12 Tm in the central region($\eta < 1.5$). The flux is closed in the iron of the yoke, where muons at $\eta = 0$ cross about 1.5 m of iron saturated with a magnetic field of 2 T providing a bending power of 3 Tm. The bending in the iron has opposite sign than the bending in the solenoid.

In ATLAS the tracks are bent in the $r - z$ plane while in CMS they are bent in the $r - \phi$ plane. When reconstructing the muon trajectory, CMS profits from the very narrow beam spot in the $x - y$ plane by constraining the track to pass through the beamline. The bending power of CMS decreases rapidly as function of η for $\eta > 1.5$, and the coverage of CMS is limited to $\eta < 2.4$. The coverage of ATLAS is slightly larger ($\eta < 2.7$) with large bending power. A comparison of the bending powers of ATLAS and CMS as a function of the pseudorapidity is shown in figure 2.

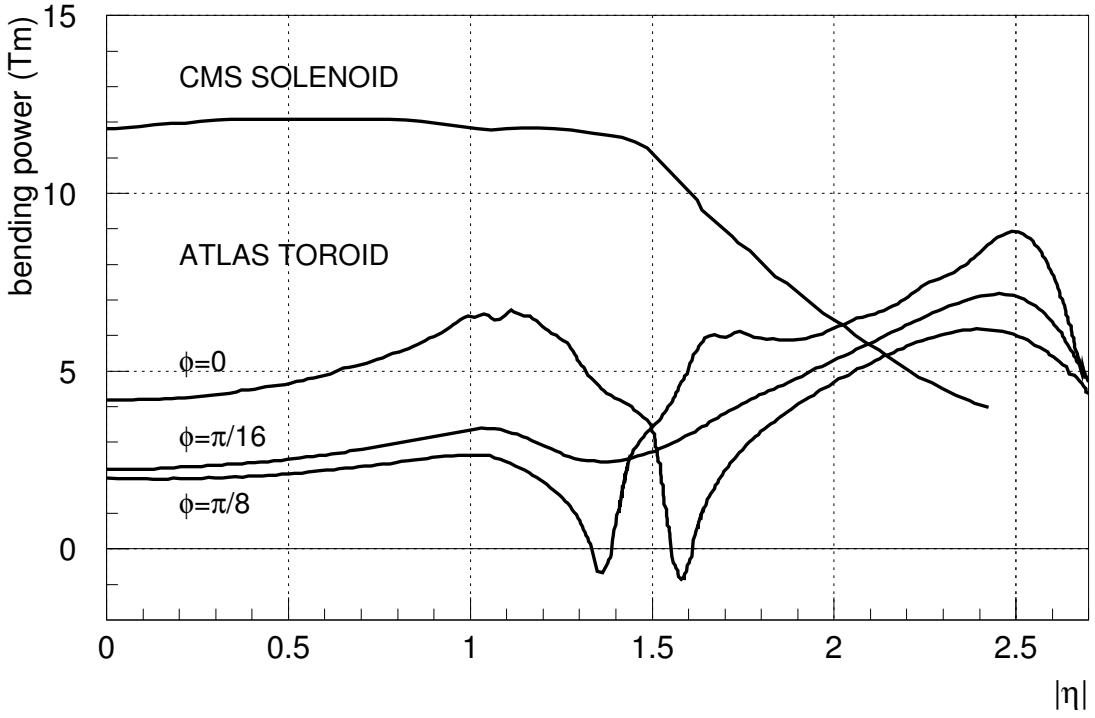

Figure 2. Bending power of the ATLAS toroid [12] and the CMS solenoid [14] fields as function of pseudorapidity [15]. The eight coils of the ATLAS barrel toroid ($|\eta| < 1.5$) are positioned at $\phi = \pi/8 + n/4$. The eight coils of the ATLAS end-caps toroid ($|\eta| > 1.5$)are positioned at $\phi = n/4$.

The CMS muon spectrometer is shielded by the iron of the magnet and is more robust against the background induced by radiation in the cavern. It suffers however from electromagnetic background in the chambers due to showering in the iron induced by muon bremsstrahlung which is relevant for muons above several hundreds GeV [10].

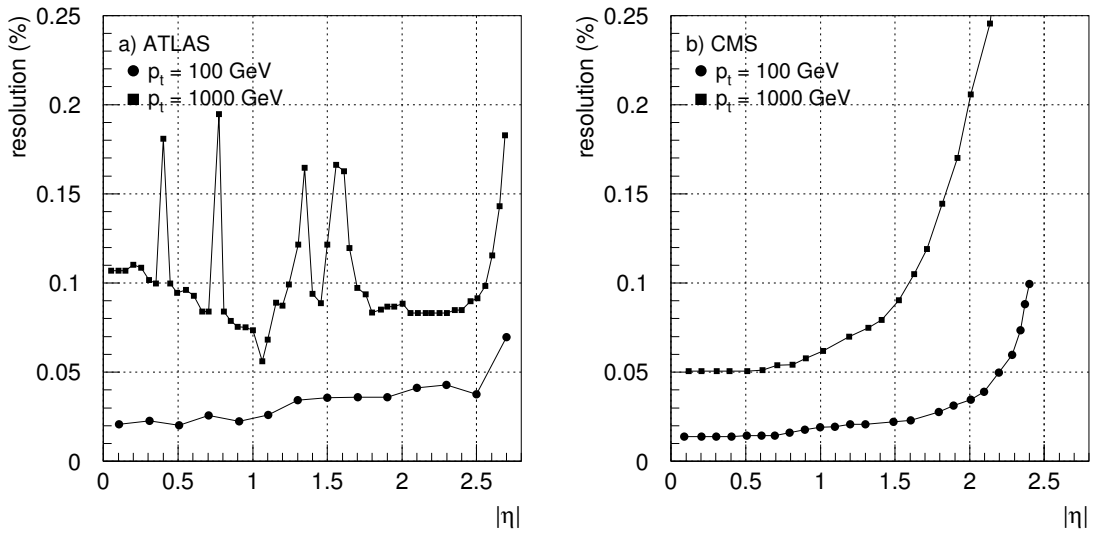

Figure 3. Relative momentum resolution as function of η for 2 different values of transverse momentum. a) ATLAS simulation: the points at $p_{\rm t}$=100 GeV [16] show the combined performance using also the inner tracker; the points at $p_{\rm t}$=1000 GeV [2] show the stand-alone performance of the muon spectrometer. b) CMS simulation showing the combined performance of the muon spectrometer and the inner tracker [3].

ATLAS tracks muons in air. A simple calculation using formula (2.4) with 3 points, the average bending power of 3 Tm and a track length of 4.5 m shows that a position resolution of 45 μm is needed to achieve a momentum resolution of 10% at 1 TeV. Since the effect of the multiple scattering is small, the momentum resolution decreases linearly with momentum.

The precision tracking of muons in ATLAS is done using Monitored Drift Tubes (MDT): tubes with outer diameter of 30 mm and featuring an average resolution of 80 μm are arranged in multilayer chambers to improve resolution and to provide redundancy. Each chamber provides a measurement of the track position with an error of about 40 μm and of the track direction with an error of about 3×10^{-4} rad. In the very forward region (see figure 1), where high counting rate is expected, the precision measurements in the first layer are provided by Cathode Strip Chambers with a resolution of 80 μm.

The momentum resolution of the ATLAS muon spectrometer can only be achieved if the relative positions of the individual chambers are known with adequate precision. Formula (2.5) with a bending power of 3 Tm and a track length of 4.5 m shows that a track of 1 TeV $p_{\rm t}$ has a sagitta of ~ 500 μm. Relative alignment of the three chambers at the level of ~ 50 μm yields a systematic uncertainly of the momentum equal to the statistical error. Given the large dimensions of the spectrometer, the position of the chambers must be continuously monitored to correct the coordinates measured by the chambers. The procedure is discussed in section 5. The precise measurement of the

momentum requires the knowledge of the complex map of the magnetic field (see figure 2) to few tens of Gauss at each point of the huge volume of the detector, 22 meters in diameter and 42 meters in length.

The tracking in the muon spectrometer of CMS is less demanding. In the barrel muons are tracked by four super-layers (see figure 1) consisting of several Drift Tubes (DT) with maximum drift length of 2 cm and space resolution of about 200 μm. Each super-layer provides a measurement of the track position with an uncertainty of about 100 μm and of the track direction with an uncertainty of about 1×10^{-3} rad. Cathode Strip Chambers (CSC) are used in the two end-caps to cope with the large magnetic field and high rate. The center of gravity of the strips provides space points with a resolution better than 200 μm and an angular resolution of 10×10^{-3} rad.

In CMS the material thickness between the interaction point and the first muon chamber amounts to about 120 radiation lengths, and muons have to cross an additional 100 radiation lengths in the yoke before reaching the last muon station [13]. The possibility to constraint the track to the interaction vertex allows CMS to exploit the large bending power of the solenoid. The angle between the muon track and radial direction at the exit of the solenoid is half of the bending angle computed with formula (2.2). A simple calculation using formula (2.6) shows that multiple scattering limits the measurement of the momentum from the direction of the track in the first muon station to about 10% for momenta below few hundred GeV. The evaluation of the momentum from the muon trajectory in the muon system alone (i.e. without the vertex constraint) is less precise. A simple calculation using formula (2.7) gives a momentum resolution of about 20%.

The momentum resolutions of ATLAS [12] and CMS [3] are derived using a full detector simulation including material effects, alignment and realistic simulations of the resolution of the detectors. Figure 3 shows a comparison of the momentum resolution as a function of η for muons with $p_{\rm t}$ 100 GeV and 1 TeV. While in CMS the resolution diverges above $|\eta| \sim 2$, ATLAS features a resolution that is roughly constant up to $|\eta| \sim 2.5$; in the region $|\eta| < 1$ CMS has a resolution at 1 TeV that is about a factor of 2 better than the corresponding resolution at ATLAS. The ATLAS plot shows also the effect of the transition region between barrel and end-cap toroids at $|\eta| \sim 1.5$.

The separate contributions of the muon spectrometers and of the inner trackers are shown in figures 4, where the muon transverse momentum resolution of ATLAS and CMS is plotted as a function of $p_{\rm t}$ in different angular regions. The figures show that the ATLAS muon system provides a stand-alone precise measurement for momenta above 100 GeV. The CMS muon system has an almost constant momentum resolution around 10% and the precise determination of the momentum is provided by the inner tracker alone up to momenta of several hundred GeV.

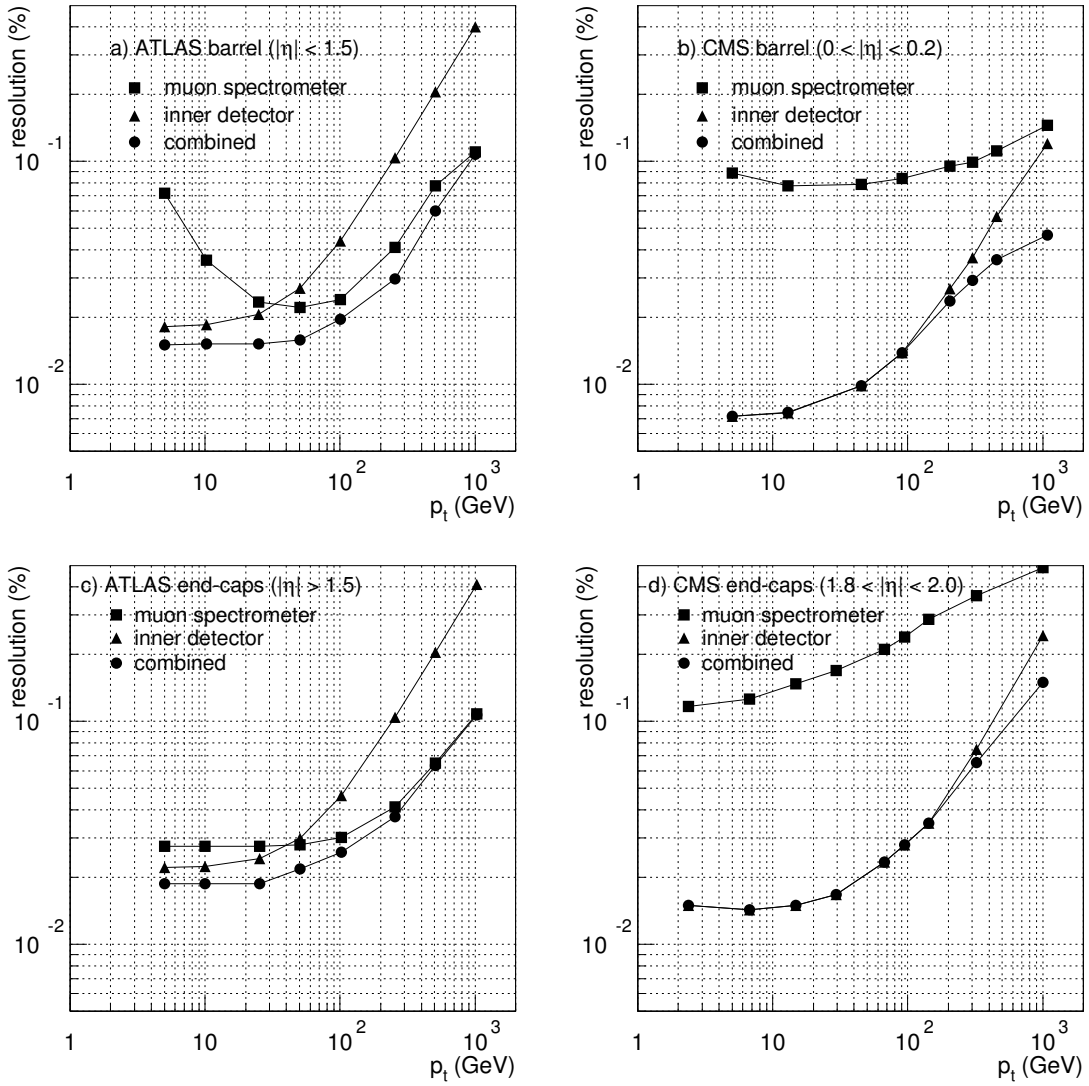

Figure 4. Relative momentum resolution as a function of the muon transverse momentum showing the stand-alone resolution of the muon systems, the stand alone resolution of the inner tracker and the combined resolution. a) and c) ATLAS [2, 17] for $|\eta| < 1.5$ and $|\eta| > 1.5$ respectively. b) and d) CMS [3] for $0 < |\eta| < 0.2$ and $1.8 < |\eta| < 2.0$ respectively;

4.2. Central tracking systems

The central trackers of ATLAS [18] and CMS [19] are similar in size and features [20]. They are located in the central part of the detector surrounding the beam pipe and are about 2 meters in diameter and 6 meters in length. They cover the angular range $|\eta| < 2.5$ and are both immersed in a solenoidal magnetic field which is 4 T and 2 T for CMS and ATLAS respectively. While the field in CMS is very uniform, the ATLAS field is not since the length of the solenoid is slightly smaller than that of the tracker.

In both trackers the innermost detector layers are built with silicon Pixels (see sec.4.3) and the intermediate layers with silicon strips detectors with high strip density.

The inner silicon strip detectors provide high resolution measurements (~ 25 μm). The barrel of ATLAS is located between $r = 30$ cm and $r = 50$ cm and provides eight measurements (4 $r-\phi$ and 4 stereo with 80 μm pitch) while that of CMS is located between $r = 20$ cm and $r = 50$ cm and provides six points (4 $r-\phi$ and 2 stereo with 80 μm pitch). The technology used for the outer layers is different: CMS uses silicon strip detectors with coarse pitch providing eight precise measurement points (~ 50 μm) between $r = 60$ and $r = 110$ cm, while ATLAS uses a Transition Radiation Detector with 4 mm diameter gas straw tubes providing 35 points with ~ 170 μm resolution [21, 22] located between $r = 55$ and $r = 105$ cm.

The most stringent design constraints for the trackers are the high granularity and readout speed needed to cope with the large rate of charged particles (see section 3). The ATLAS silicon strip tracker has about 6 million channels and the CMS strip tracker has about 10 million channel. At design luminosity the occupancy in the innermost silicon strip layer is $\sim 1-2\%$ while the occupancy in the ATLAS TRT varies from 13% to 38% [18, 23].

The trajectories are built starting from inner part of the trackers (pixel or strip layers) and are propagated toward the external layers. The number of compatible hits found on the next layer depends on many factors like the lever arm between the last and the next layer and the number of hits already assigned to the trajectory and their resolution. Once four or five silicon hits are assigned to the trajectory the number of spurious hits found on the next layer is negligible also for high $p_{\rm t}$ jets [3].

In ATLAS tracks formed with hits from silicon detectors are extrapolated to the TRT where straws are associated to the tracks if they satisfy tight cuts on the straws residuals and on the ratio of found to expected straws in order to limit high luminosity ocuupancy effects [24]. The collaboration plans to implement a second-stage pattern recognition starting in the TRT using hits not assigned to tracks and proceed inward to reconstruct conversions and other vertices in the outer layers [25]. The TRT also provide electron identification capability improving the hadron/jet rejection power of the ATLAS detector [18].

The huge number of front-end electronics channels located on the detectors in the limited volume requires high power ($\sim 60-70$ kW) and high cooling power resulting in large material budget. Figure 5 shows a typical material distribution as a function of the pseudorapidity with the breakdown in the different parts composing the detector. The total amount of material can be as high as $\sim 40\%$ of a radiation length at $\eta = 0$, rising above 100% of a radiation length at critical values of η where the effect of the detector services concentrated at the end of the barrel and at the end of the end-caps is clearly visible. The material budget of the sensitive part of the detector is less than 10%.

The large amount of material spread along the trajectory of electrons affects the measurement of their energy in the calorimeter. Hadrons are affected as well: $\sim 20\%$ of them interact within the volume of the tracker. The high radiation dose integrated during the lifetime of the detectors will degrade their response, which is especially

important for the detectors close to the interaction point.

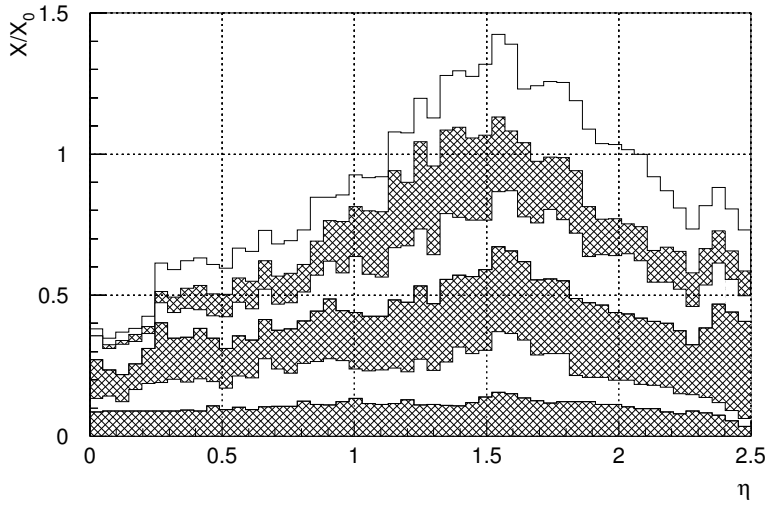

Figure 5. Typical distribution of the material in the central tracker as a function of η; the different curves show the contributions of the different functional parts of the system. Bottom to top: active sensors, front-end electronics, support structures, cooling system, cables, other structures.

Since the trackers are very massive, the momentum resolution at low momentum is limited by multiple scattering. Formula 2.7 shows that in this regime the dependence of the momentum resolution on the material budget is weak and that the resolution scales linearly with the magnetic field. Inserting in formula 2.7 the numerical values of 0.4 radiation lengths and 4(2) Tm bending power, one obtains a momentum resolution at $\eta = 0$ of 0.8% in CMS and 1.6% in ATLAS.

The momentum resolution of the inner trackers shown in figures 4 a) and b) can be roughly parametrized at $\eta = 0$ in ATLAS [2] and CMS as:

$$\frac{\delta p_{\mathrm{t}}}{p_{\mathrm{t}}} = (1.6 \oplus 0.034 \times p_{\mathrm{t}}(\mathrm{GeV}))\% \tag{4.1}$$

and

$$\frac{\delta p_{\mathrm{t}}}{p_{\mathrm{t}}} = (0.8 \oplus 0.015 \times p_{\mathrm{t}}(\mathrm{GeV}))\% \tag{4.2}$$

for $p_{\mathrm{t}} < 500$ GeV respectively. Comparison of these parametrizations with formula 2.4 shows that this momentum resolution is obtained with an average spatial resolution on silicon of ~ 30 μm. Since the two trackers have similar dimensions, resolutions and material budget, the two parametrizations scale roughly linearly with the magnetic field. In both detectors the multiple scattering is the main contribution to the momentum resolution for $p_{\mathrm{t}} < 50$ GeV at η=0.

4.3. Vertex detectors

ATLAS and CMS have built pixel vertex detectors [26, 27] providing space point measurements which allow an efficient and robust pattern recognition. ATLAS optimizes

the position resolution in the plane perpendicular to the magnetic field (along the z axis) using a rectangular pixel of 400×50 μm^2, while CMS optimizes the resolution in both coordinates simultaneously with a pixel of 150×100 μm^2.

The minimum pixel size is determined by the surface occupied by a front-end electronics cell on a custom ASIC connected to the sensor using *bump bonding* [28] done either with Indium or Pb/Sn. Both experiments have similar geometries: barrel layers closed by end-cap disks. The main parameters of the two layouts are summarized in table 1. Using the track density parametrization $40/r^2$ tracks per unit surface (see section 3) the occupancy of the innermost layer is $\sim 3.1 \times 10^{-4}$, almost identical for the two designs.

Table 1. Geometry of the ATLAS and CMS pixel detectors

	ATLAS	CMS
Barrel layers	3	3
Barrel layers radii (cm)	5.1, 8.9, 12.3	4.4, 7.3, 10.2
Barrel length (cm)	77	53
Number of disks	2×3	2×2
Disks positions along z (cm)	$\pm 49.5, \pm 58, \pm 65$	$\pm 34.5 \pm 46.5$
Disks inner/outer radius (cm)	8.9/15.0	6.0/15.0
Pixel size ($r-\phi \times z$, μm)	50×400	100×150
Sensor thickness (μm)	250	285
Module dimensions ($r-\phi \times z$, mm)	16.4×60.8	16.2×66.3
Total number of pixels	80×10^6	66×10^6
Acceptance	$\lvert\eta\rvert < 2.5$	$\lvert\eta\rvert < 2.5$

ATLAS and CMS [29, 30] have built the detectors using a double sided process: n silicon as bulk material is used, on which n^+ pixels are implanted, while a p implant on the back-side forms the pn junction. The choice of a n^+ on n sensor requires pixels insulation, implemented using the *p-spray* technique [31].

The spatial resolution is mainly determined by the pixel cell size and by the degree of charge sharing between two adjacent pixels. Charge sharing depends a) on intrinsic sensor properties (e.g. inter pixel capacitance and pixel to back-plane capacitance, diffusion), b) on parameters related to the electronic readout like the threshold, and c) on operational conditions like the reverse bias operating voltage that determines the depth of the fully depleted region in the detector and the mobility of the electrons. The actual sharing is established by the crossing angle θ of the charged particle trajectory with the normal to the sensor, and by the Lorentz angle Θ_{L} due to the $\boldsymbol{E} \times \boldsymbol{B}$ force on the charge carriers inside the detector: they determine the width of the electron swarm collected on the pixel plane $W = D|\tan\Theta_{\mathrm{L}} - \tan\theta|$, where D is the active sensor thickness (i.e. the depleted region).

The minimum of the resolution as function of the track angle is obtained [32, 33] when the width W of the electron swarm is equal to the pixel pitch: in this condition

one has the optimal sharing of the charge between only 2 adjacent pixels and a charge interpolating algorithm gives the best accuracy. ATLAS and CMS claim resolutions as low as 4 μm can be achieved for the optimal crossing angle [32, 33].

Due to the different magnetic fields, the Lorentz angle in the ATLAS pixel detector is 12° [32], while in CMS it is 24° [33], both at the nominal polarization potential V_d= 150 V at the beginning of LHC operation. To compensate for radiation damage, the voltage will rise up to $\sim$ 600 V at the end of sensors lifetime with reduction of the mobility and reduced (and possibly not uniform within the sensor) Lorentz angles of 4° for ATLAS and 8° for CMS.

ATLAS has chosen a barrel layout such that the normal to the sensor makes an angle of $\sim 20°$ with respect to a radius crossing the center of the module: the angle formed by a stiff track originating from the interaction point with the normal to a sensor of the innermost layer is approximately $\theta = 20° \pm 9°$.

CMS has chosen to mount the barrel modules perpendicular to the radius and in their case the range of the track crossing angle is $\theta = \pm 10°$. For not irradiated sensors the above figures correspond to a range of electron swarm widths $W = 42 \pm 42$ μm for ATLAS and $W = 125 \pm 50$ μm for CMS; in both cases the average width matches adequately the pixel pitch and both collaborations quote an average resolution ~ 10 μm in $r - \phi$. In the $r - z$ view the expected resolutions are ~ 100 μm in ATLAS and ~ 20 μm in CMS.

During operation at LHC the radiation damage modifies the working conditions of the detector. The effective p doping increases, eventually leading to a *type inversion*, after which the junction moves from the back-side to the pixels. The depletion voltage also increases and can become so high that one has to consider the operation of the detector not fully depleted.

The mechanical structure has to provide good position stability that matches the spatial resolution with the minimum amount of material; it must also provide adequate cooling to remove the heat (some watt per module) produced by the front-end electronics and the sensor leakage current and eventually keep the detector at low temperature to reduce reverse annealing (- 6° C for ATLAS and -10 ° C for CMS). The total material budget in the barrel for normal incidence is around 8% X_0.

At low momenta the precision of the impact parameter depends mainly on the material between the interaction point and the first layer (the beam-pipe), and on the material of the first layer itself. The multiple scattering caused by the two material layers modifies the angle of the trajectory and causes an uncertainty of the impact parameter when the track is extrapolated back at the origin. Assuming beam pipe and first layer at a radii r_b and r_1, causing a random scattering θ_b and θ_1 respectively, the contribution to the impact parameter uncertainty is $\sigma_{ip} = r_b\theta_b \oplus r_1\theta_1$. The beryllium beam pipe of 0.45% X_0 at a radius of 32 mm contributes an error of approximately 30 μm at 1 GeV. The first layer has an equivalent thickness of about 2.5% X_0 and contributes 110 μm for ATLAS (r_1=5.1 cm) and 95 μm for CMS (r_1=4.4 cm). This is the dominant contribution at low momenta.

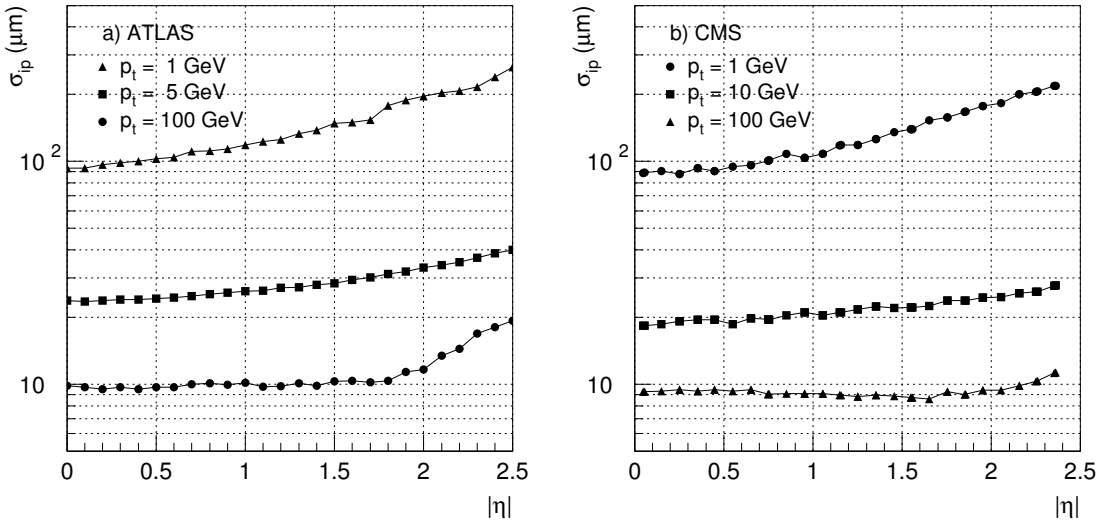

Figure 6. Impact parameter resolution of the ATLAS [2, 34] and CMS [3] detector as function of η for different values of the transverse momentum. The middle curves are at $p_{\rm t} = 5$ GeV for ATLAS and $p_{\rm t} = 10$ GeV for CMS.

At large momenta the resolution on the impact parameter is dominated by the position resolution of the first plane of the tracker and its distance from the interaction point. The measurement can be modeled [8] as the extrapolation to the origin of a track of known momentum and direction (measured by the N outermost planes) and constrained by the position measured by the first plane placed at $r \sim 4-5$ cm from the primary vertex.

The momentum resolution of ATLAS and CMS trackers is $\delta p/p^2 \sim O(10^{-4})$ GeV^{-1} which corresponds to $\delta R/R^2 \sim O(10^{-4})$ m^{-1}: the effect on extrapolation over distances of the order of 5 cm is negligible. The error $\sigma_{\rm b}$ on the slope varies from 0.06 mrad to 0.1 mrad going from 50 GeV to 1 TeV and when extrapolated over 5 cm contributes an error from 3 to 5 μm to be compared with the resolution of the first plane $\sim 10\mu$m. The impact parameter resolution for different momenta as function of the pseudorapidity is shown in figure 6.

5. Alignment

The intrinsic resolution of the tracking detectors is usually better than the precision of the detector assembly. Moreover, the position of the detectors may change with time due to magnetic field and environmental effects like change of temperature. Alignment procedures are used to measure and monitor the position of the detectors over time to recover the intrinsic resolution of the measurements of the particle trajectories. These procedures combine the use of dedicated optical alignment systems based on beams of laser or LED light and the fit of the corrections from the nominal to the real positions using a (large) set of reconstructed trajectories of particles [35]

The alignment with optical systems is based on a network of on-line measurements of the relative positions between light sensitive detectors which are precisely mounted on the particle detectors. The number of measurements largely exceeds the degree of freedoms of the overall system and the position of the particle detectors are computed as free parameters in a fit to the whole set of measurements. The accuracy of the single measurement is typically few microns and systematic effects dominate the alignment precision.

The track-based alignment computes the corrections from the nominal to real position of detectors with a linear least square fit. This fit minimizes the residual between the predicted and measured positions of hits belonging to a large set of tracks as a function of correction parameters. The systematic errors of this method are usually small, however large sets of tracks are needed to achieve the required precision. The method is not robust against fast movements of the detectors, where fast refers to the time needed to collect the relevant integrated luminosity.

The ATLAS and CMS collaborations have estimated misalignment scenarios [2, 3] for the first data taking. As an example, the impact of the misalignment can be seen in figure 7 on the left where the transverse momentum resolution obtained in CMS for two misalignment scenarios is compared with the resolution obtained with ideal alignment.

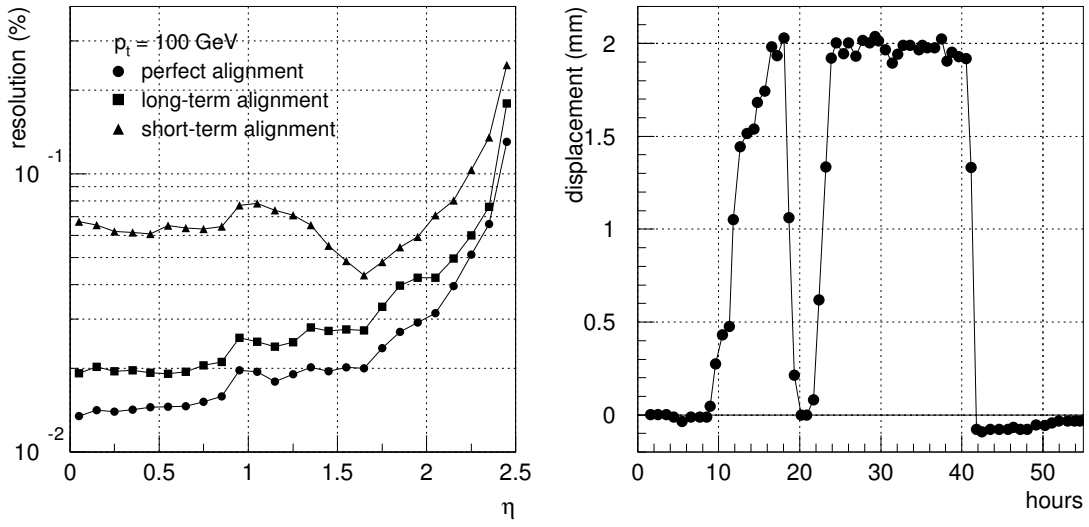

Figure 7. Left: effect of two different misalignment scenarios [3] achievable in CMS with an integrated luminosity smaller than 1 fb^{-1} and larger $1 \ldots 5$ fb^{-1} on the transverse momentum resolution as a function of the pseudorapidity η. The ideal resolution is shown as reference. Right: ATLAS barrel toroid, displacement in mm of the upper coil versus time on November 18$^{\text{th}}$ and 19$^{\text{th}}$ 2006. The time origin starts at 00:00 of November 18$^{\text{th}}$. Two peaks can be seen, corresponding to 2 different ramp ups. The end of the second peak corresponds to a fast quench of the toroid system.

The track-based alignment is faster when the extrapolation of the measured trajectory on the detector layer has an intrinsically small statistical error. This is the case for the inner tracking detectors where there are many measurement layers separated

by small extrapolation distance and with limited material in between layers, resulting in small multiple scattering errors. The muon systems instead have less measurement points with large extrapolation distance and in some cases large multiple scattering in between layers. Precise knowledge of the magnetic field map is needed for the track extrapolation. This induces systematic errors in the track-based alignment which are usually smaller for the inner detectors where the magnetic field is constant and larger for the muon systems where the magnetic field varies along the trajectory of the particle.

Optical alignment methods require free line of sight between optical detectors, which is a limitation especially important for the inner trackers, where the particle detectors are densely packed in nearby layers and many services have to be routed. Therefore, the inner trackers are aligned using track-based procedures while optical systems are used to monitor a limited number of degrees of freedom, providing valuable information on the stability of the detectors.

The track-based alignment uses mainly tracks originating from the interaction point which are not able to constrain all parameters. A number of correlated displacements of the detector layers [36] do not produce at first order a variation of the chi-square of the fit like, for example, a correlated shift along z as function of r. These correlated movements are constrained using different data samples like cosmic rays and muons from the beam halo and also applying constraints like common vertex in multi-track events and mass constraints on the decay products of known resonances.

The large muon systems are prone to temperature effects and to movements induced by ramping the magnets up and down. In ATLAS and CMS the muon chambers move by several millimeters when the magnets are being turned on, with a reproducibility of about 1 mm, larger than the intrinsic resolution of the detectors. Figure 7 on the right shows the displacement of one of the coils of ATLAS during the test of their magnet as measured by the muon alignment system.

The muon systems of ATLAS and CMS are aligned mainly with optical systems. The specifications are somewhat more relaxed in CMS, which tracks in iron, requiring an alignment precision of the order of 100 μm, compared to ATLAS which tracks in air and requires better than 50 μm alignment accuracy. ATLAS uses a sophisticated optical system [37–39] to monitor the relative position of the components of the chambers to a precision of $\sim$ 10 μm and the relative position of the chambers to a precision of $\sim$ 30 μm.

The impact of the alignment errors on the momentum resolution of the ATLAS Muon Spectrometer can be seen in figure 8, where the separate contributions of the chambers resolution, chambers alignment, multiple scattering, and energy loss fluctuations are also shown. Here the multiple scattering contribution is evaluated as the quadratic difference of the calculations performed with and without the material of the spectrometer.

Depending on the number of independent detectors to be aligned, the simultaneous fit of a large number of parameters can be computationally challenging. In some cases the alignment problem can be factorized into a number of smaller and weakly correlated

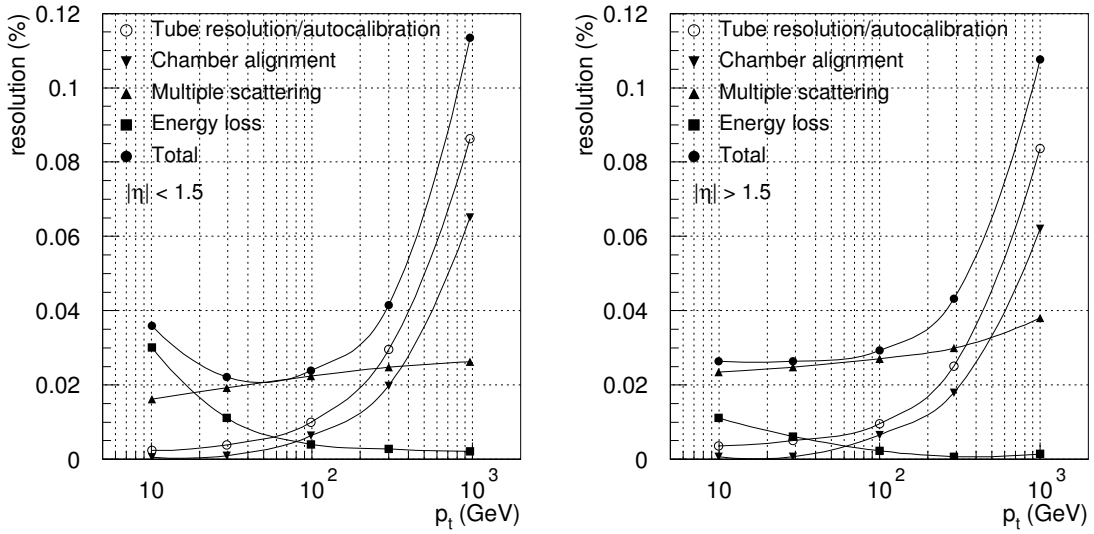

Figure 8. Breakdown of the contribution of the different effects to the momentum resolution as a function of the muon transverse momentum for the ATLAS muon spectrometer [12]; left: barrel ($|\eta| < 1.5$); right: end-caps ($|\eta| > 1.5$.

problems. This is the case in the ATLAS end-cap alignment which comprises about 10,000 fitted parameters in total and can be factorized in 864 partial fits of 9 or 12 parameters each, and two global fits of 384 parameters each, reducing the computational time by several orders of magnitude.

This factorization cannot be applied to inner trackers where the number of strongly correlated detectors is large. The most complex case is the CMS inner silicon tracker which has more than 15000 modules resulting in about 100.000 parameters to be simultaneously fitted in the track-based alignment. Using conventional methods involving matrix inversion becomes extremely difficult because of computing time and numerical precision. Novel alignment algorithms have been developed replacing the matrix inversion by a fast numerical solver [40], or using the Kalman filter approach where the alignment is updated iteratively and the matrix inversion is performed only on a much smaller matrix size [41].

6. The muon trigger systems

The muons spectrometers also provide fast trigger with a p_{t} cut. Typical thresholds are in the region of 20 GeV and the momentum resolution defines the sharpness of the threshold.

ATLAS uses dedicated detectors for the trigger: Resistive Plate Chambers in the barrel and Thin Gap Chambers in the end-caps (see figure 1). The trigger is provided constructing a search road centered around the trajectory of an infinite momentum track originating from the nominal interaction vertex and passing through the hits measured on a preferential plane used as pivot. The width of the search road is determined by

the muon momentum used as threshold and the trigger uses predefined coincidence patterns stored in a Coincidence Matrix. In the barrel the distance between the pivot plane (middle plane) and the uppermost plane is of the order of 2.5 m, which corresponds to approximately half the overall bending power $\int B\mathrm{d}\ell \sim 1.8$ Tm. Formula 2.2 yields that a 20 GeV muon is deflected by an angle $\theta \sim 0.013$ rad, which corresponds to a transverse displacement of ~ 3.2 cm over 2.5 m. This displacement can be compared with the 1 cm resolution of the RPCs. In the end-caps there are regions in which the bending power can be as low as $\sim$2 Tm (see figure 2) and the lever arm is also smaller ($\sim$ 0.5 m) because the chambers are placed outside the magnet cryostat. The corresponding transverse displacement is ~ 0.8 cm: to obtain a sharp efficiency curve the chambers in the end-caps must have better resolution than those of the barrel.

In CMS the trigger information is provided by the Drift Tubes in the barrel and by the Cathode Strips Chambers in the end-caps, complemented by Resistive Plates Chambers both in the barrel and in the end-caps (see figure 1). The trigger system of CMS combines the information of the three detectors and their quality estimators to provide the best compromise between efficiency and background rejection. The electronics measurement of the Drift Tubes provides the track position with an error of about 1.5 mm and of the track direction with an error of about 6×10^{-2} rad. The Cathode strip chambers measure the track position at trigger level with an accuracy of 1-2 mm. The segmentation of the RPCs varies between 10 mm at large η and low radii to about 40 mm at the outer radius. In the DT and CSC the trigger is provided finding muon segments in each chamber which are later joined together. The transverse momentum is measured using the difference between the ϕ coordinates of the two innermost layers and assuming the nominal interaction vertex. The trigger in the RPC is based on the spatial and time coincidence of hits in four RPC muon stations, assuming the nominal interaction vertex.

The multiple scattering angle of a 20 GeV muon crossing the 120 radiation length the first super-layers of the CMS barrel is 7 mrad (see formula 2.6) while the angular resolution of the muon track candidate is about 10 mrad. The momentum resolution at trigger level at 20 GeV is less than factor of 2 worse than the resolution shown in figure 4b.

The correct calculation of the efficiency curves can performed only with a full detector simulation which properly takes into account the correct resolution of the detectors and other effects like field inhomogeneities, multiple scattering, energy loss fluctuations in the calorimeters, size of the interaction region that all contribute to smear the edge of the efficiency curve.

Figure 9 shows the muon level 1 trigger efficiency as a function of the muon momentum. The curves also include the effect of the geometrical acceptance which are especially important in the open air toroidal magnet, which requires a complex support structure that affects the geometrical acceptance of the ATLAS muon system: depending on the number of hits required, the acceptance varies from $\sim$ 89% to $\sim$ 100%. The transverse momentum spectra of muons fall very rapidly and the trigger

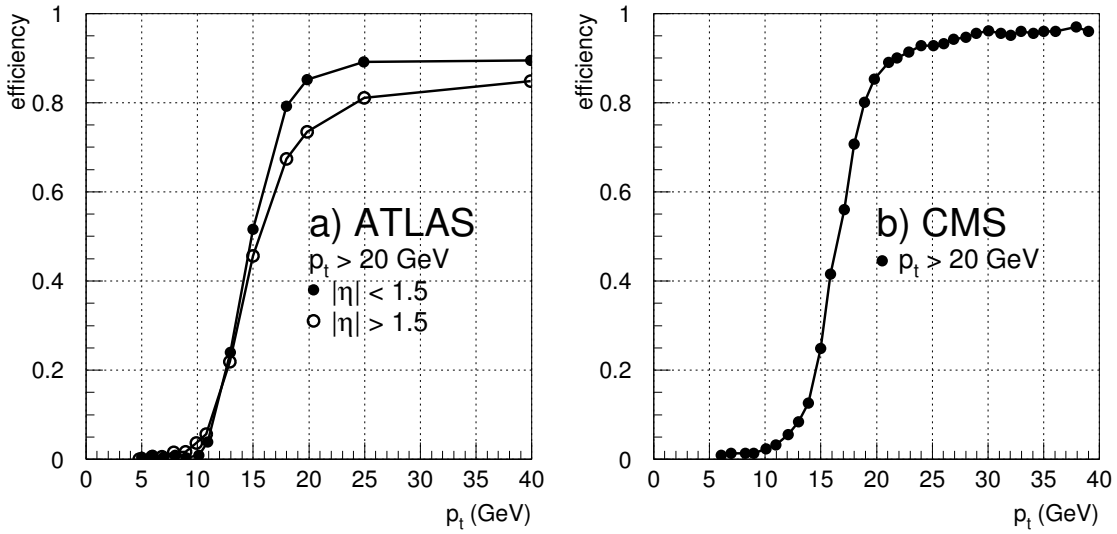

Figure 9. Efficiency of the level 1 muon trigger as a function of the muon $p_{\rm t}$ for a 20 GeV threshold setting; a) efficiency for the ATLAS experiment [12] for the barrel ($|\eta| < 1.5$ and the end-cap ($|\eta| > 1.5$). b) efficiency for the CMS experiment [42] for $|\eta| < 2.1$.

rate depends strongly on the steepness of the efficiency curve near the threshold. The curves shown in figure 9 are similar and the experiments quote a Level 1 trigger rate of $\sim$ 4-5 KHz at 20 GeV and at the LHC design luminosity $1 \times 10^{34}{\rm cm}^{-2}{\rm s}^{-1}$.

7. Conclusions

The tracking systems of ATLAS and CMS are designed to cope with the harsh conditions of the LHC interaction region. The momentum of muons can be precisely measured up to few TeV and the precision of the vertex systems is well matched to identify long lived particles assuring efficient b-tagging. We conclude this review with two examples showing how tracking performance is important for discovery of new physics and for studies of Standard Model physics.

Discovery of a Z' of 1 TeV at LHC through its decay into $\mu^+\mu^-$. For $\mu^+\mu^-$ invariant masses of 1 TeV the fraction of Drell-Yan events with both muons in the acceptance ($\eta < 2.5$) is about 80% and the trigger efficiency is also large, in excess of 90%. Typical selection efficiencies for this simple signature are also large [43]. The discovery potential for a new Z' resonance decaying into $\mu^+\mu^-$ depends on muon momentum resolution, the main background being the irreducible Drell-Yan process. Figure 10a shows an example of a CMS start-up analysis with a not yet fully aligned detector (see section 5). With the resulting momentum resolution, 30 pb^{-1} of data are sufficient for a 5 sigma signal.

Selection of very pure samples of top. At LHC top quarks are copiously produced in pairs via gluon fusion and can be selected at trigger level through the semi-leptonic decay of one of them. Topology based analysis can select samples with purity larger

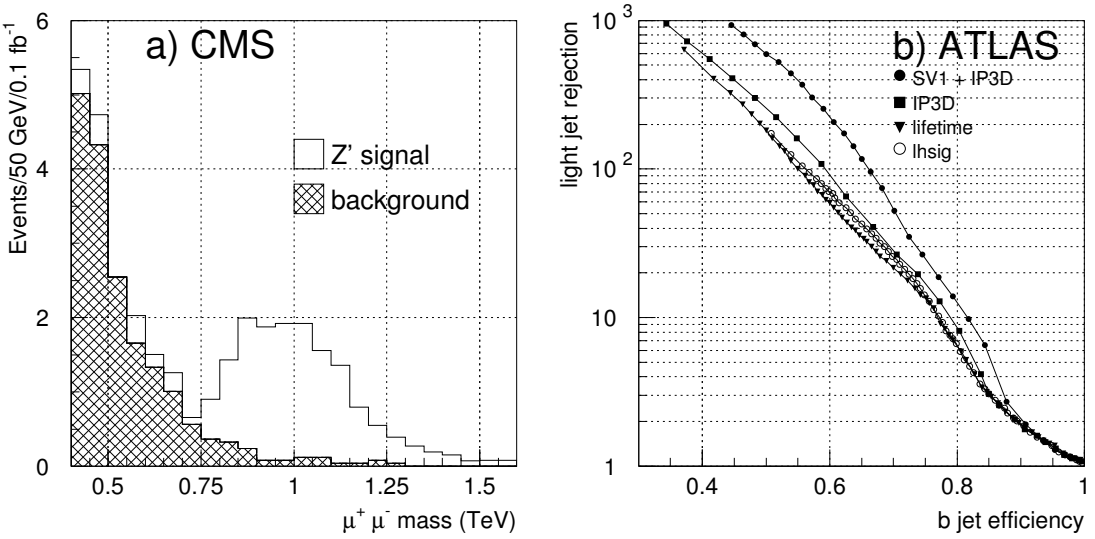

Figure 10. a) Histogram of the $\mu^+\mu^-$ invariant mass for 1 TeV Z' plus background (open histogram) and for background only(shaded histogram) for events selected assuming the it first data alignment scenario of CMS (see section 5). The number of events per bin is normalized to an integrated luminosity of 100 pb^{-1} [43]. b) ATLAS b-tagging: light jet rejection as function of b tagging efficiency in semileptonic $t\bar{t}$ events for different tagging algorithms [44].

than 10 and efficiency in excess of 25% [45, 46]. Those events have 4 jets: three of them originating from the hadronically decaying top while one is the b-jet from the leptonically decaying top. b-tagging can be used to assign flavor to the jets.

Since lifetime distributions are peaked at zero, b-tagging based selections are not efficient but can be used to select very pure samples. Typical tagging efficiency vs light jet rejection is shown in figure 10b. The purity of the sample is traded against efficiency and can be tuned selecting the appropriate b-tag cut: for example purities in excess of 60 can be achieved for precise measurement of the top mass [46]. b-tagging also plays a central role in the search of any non standard model interaction with top quarks in the final state [47].

Acknowledgments

We are grateful to our colleagues of the ATLAS and CMS collaborations for many interesting discussions on tracking. The original figures have been digitized using the open source program *Engauge Digitizer* 4.1 written by Mark Mitchell. We thank Philipp Schieferdecker for his careful reading of the paper.

References

[1] Cvetic M and Langacker P 1996 Implications of Abelian Extended Gauge Structures From String Models *Phys. Rev.* D **54** 3570-9

Cvetic M and Langacker P 1996 New Gauge Bosons from String Models *Mod. Phys. Lett.* A **11** 1247-62

Leike A 1999 The phenomenology of extra neutral gauge bosons *Phys. Rept.* **317** 143-250

Hill C T and Simmons E H Strong dynamics and electroweak symmetry breaking 2003 *Phys. Rept.* **381** 235-402

Han T, Logan H, McElrath B and Wang L T 2003 Phenomenology of the little Higgs model *Phys. Rev.* D **67** 095004

[2] ATLAS Collaboration 1999 *ATLAS Detector and Physics Performance Technical Design Report* CERN/LHCC 99-14 CERN Geneva, 25 May 1999

[3] CMS Collaboration 2006 *CMS Physics Technical Design Report Vol 1* CERN/LHCC 06-01 CERN Geneva, 2 February 2006

[4] Billoir P 1984 Track fitting with multiple scattering: a new method *Nucl. Instrum. Methods* A **225** 352

Frühwirth R 1987 Application of Kalman filtering to track and vertex fitting *Nucl. Instrum. Methods* A **262** 444

Mankel M 1997 A concurrent track evolution algorithm for pattern recognition in the HERA-B main tracking system *Nucl. Instrum. Methods* A **395** 169-84.

[5] Frühwirth R 1997 Track fitting with non-Gaussian Noise *Comp. Phys. Commun.* **100** 1

Adam W, Frühwirth R, Strandlie A and Todorov T 2005 Reconstruction of electrons with the Gaussian-sum filter in the CMS tracker at the LHC *Journ. Phys. G - Nucl. Part. Phys.* **31** N9

Atkinson T 2006 *Electron reconstruction with the ATLAS Inner Detector* PhD thesis University of Melbourne. Melbourne, Australia 2006

[6] Frühwirth R and Strandlie A 1999 Track fitting with ambiguities and noise: a study of elastic tracking and nonlinear filters *Comp. Phys. Comm.* **120** 197-214

Speer T *et al* 2006 Robust vertex fitters *Nucl. Instrum. Methods* A **566** 149-52

[7] Bock R K, Grote H, Notz D and Regler M 1990 *Data Analysis Techniques for High-Energy Physics Experiments* (*Camb. Monogr. Part. Phys. Nucl. Phys. Cosmol.*) vol 11 Cambridge University Press Cambridge, UK 1990 p 240

[8] Blum W, Rolandi L 1993 *Particle Detection with Drift Chambers* Springer-Verlag Berlin, Germany 1993 p 201

[9] Gluckstern R L 1963 Uncertainties in track momentum and direction. due to multiple scattering and measurement error *Nucl. Instrum. Methods* **24** 381-9

[10] Bichsel H, Groom D E and Klein S R 2006 J.Phys. G: Nucl. Part. Phys. 33 **258-70**

[11] Dawson I 2000 *Review of the radiation environment in the inner detector* ATLAS note ATL-INDET-2000-006 CERN Geneva, 11 February 2000

[12] ATLAS Muon Collaboration 1997 *ATLAS Muon Spectrometer Technical Design Report* CERN/LHCC 97-2 CERN Geneva, 5 June 1997

[13] CMS Collaboration 1997 *The Muon Project Technical Design Report* CERN/LHCC 97-32 CERNGeneva, 15 December 1997

[14] CMS Collaboration 1977 *The Magnet Project Technical Design Report* CERN/LHCC 97-10 CERNGeneva, 2 May 2007

[15] Wrochna G. 1993 *Plots of the bending power* Unpublished
`http://wrochna.web.cern.ch/wrochna/GW_slides/cms/GW_cms.html#magnet`

[16] Benekos N Chr 2005 *Muon identification and reconstruction inthe ATLAS detector at the LHC* Presented at the 9th ICATPP Conference on Astroparticle, Particle, Space Physics, Detectors and Medical Physics Applications, Villa Erba, Como, Italy, 17-21 Oct 2005
`http://villaolmo.mib.infn.it/ICATPP9th_2005/`

[17] Kortner O 2006 *Muon identification in ATLAS and CMS* Talk given at the Hadron Collider Physics Symposium, Duke University Durham NC, May 22-26 2006
`http://projects-docdb.fnal.gov/cgi-bin/ShowDocument?docid=82`

[18] ATLAS Collaboration 1997 *Inner DetectorTechnical Design Report Vol 1 & 2* CERN/LHCC 97-16

CERN Geneva, 15 December 1997

[19] CMS Collaboration 1998 *CMS Tracker Project Technical Design Report* CERN/LHCC 98-06 CERN Geneva, 15 April 1998
CMS Collaboration 2000 *Addendum to CMS Tracker Project Technical Design Report* CERN/LHCC 00-16 CERN Geneva, 21 February 2000

[20] Froidevaux D and Sphicas P 2006 General-purpose detectors for the Large Hadron Collider *Ann. Rev. Nucl. Part. Sci.* **56** 375-440

[21] Akesson T *et al* 2004 Operation of the ATLAS Transition Radiation Tracker under very high irradiation at the CERN LHC *Nucl. Instrum. Methods* A **522** 25-32

[22] Akesson T *et al* 2004 ATLAS Transition Radiation Tracker test-beam results *Nucl. Instrum. Methods* A **522** 50-5

[23] Akesson T *et al* 2004 Status of design and construction of the Transition Radiation Tracker (TRT) for the ATLAS experiment at the LHC *Nucl. Instrum. Methotds* A **522** 131-45

[24] Benekos N, Clifft R, Elsing M and Poppleton A 2004 *ATLAS inner detector performance* ATLAS note ATL-INDET-2004-002 CERN Geneva, Switzerland, 2 October 2003

[25] Fleishmann S 2007 *Track reconstruction in the ATLAS experiment: the deterministic annealing filter* PhD thesis, CERN-THESIS-2007-11 pag. 32 BergischeUniversität Wuppertal Wuppertal, Germany 2007

[26] ATLAS Pixel Detector Community 1998 *ATLAS Pixel Detector Technical Design Report* CERN/LHCC 98-13 CERN Geneva, 5 May 1998

[27] CMS Collaboration 1998 *The traacker system project Technical Design Report* CERN/LHCC 98-06 CERN Geneva, 15 April 1998

[28] Alimonti G *et al* 2006 Analysis of the production of ATLAS indium bonded pixel modules *Nucl. Instrum. Methotds* A **565** 296-302
Grosse-Knetter J *et al* 2006 Experience with module-production and system tests for the ATLAS Pixel Detector *Nucl. Instrum. Methotds* A **565** 79-84
Broennimann C *et al* 2006 Development of an indium bump bond process for silicon pixel detectors at PSI *Nucl. Instrum. Methotds* A **565** 303-8
Airoldi A *et al* 2005 A chip removal facility for indium bump bonded pixel detectors *Nucl. Instrum. Methotds* A **540** 259-65

[29] Alam M S *et al* 2001 The ATLAS silicon pixel sensors *Nucl. Instrum. Methotds* A **456** 217-32

[30] Arndt A *et al* 2003 Silicon sensors development for the CMS pixel system *Nucl. Instrum. Methotds* A **511** 106-11

[31] Richter R H *et al* 1996 Strip detector design for ATLAS and HERA-B using two-dimensional device simulation *Nucl. Instrum. Methotds* A **377** 412-21

[32] Gorelov I *et al* 2002 A measurement of the Lorentz angle and spatial resolution of radiation hard silicon pixel sensors *Nucl. Instrum. Methotds* A **481** 204-21

[33] Allkofer Y *et al* 2007 *Design and performance of the silicon sensors for the CMS barrel pixel detector* submitted to *Nucl. Instr. Methods* preprint arXiv:physics/070209v1

[34] Poppleton A, Benekos N Ch, Dallison R C S and Gorfine G 2007 *ATLAS inner detector performance with the Rome-initial layout* ATLAS note ATL-INDET-PUB-2007-008 CERN Geneva, 5 May 2007

[35] Blusk S *et al* 2007 *Proceedings of the first LHC detector alignment workshop, 4-6 september 2006* CERN YELLOW REPORT 2007-004 CERN Geneva, Switzerland, 20 june 2007

[36] Golling T 2006 *Alignment of the silicon tracking detector using survey constraints* ATLAS note ATL-INDET-PUB-2006-001 CERN Geneva, 6 March 2006

[37] Machefert F, Guyot C, Schuller JP and Schune P 2001 *Calibration of a RASNIK system for the ATLAS Muon Spectrometer* ATLAS note ATL-MUON-2001-10 CERN Geneva, 19 November 2001

[38] Blum W, Kroha H, Widmann P 1995 A novel laser-alignment system for tracking detectors using transparent silicon strip sensors *Nucl. Instrum. Methotds* A **367** 413-7

[39] Blum W, Kroha H, Widmann P 1996 Transparent silicon strip sensors for the optical alignment of particle detector systems *Nucl. Instrum. Methotds* A **377** 404-8

[40] Schleper P *et al* 2006 *Software alignment of the CMS tracker using MILLEPEDE II* , CMS note CMS-NOTE-2006-011 CERNGeneva, 20 January 2006

[41] Widl E, Frühwirth R and Adam W 2006 *A Kalman filter for track-based alignment* CMS note CMS-NOTE-2006-022 CERN Geneva, 30 January 2006

[42] CMS Collaboration 2002 *Data Acquistion and High Level Trigger Technical Design Report* CERN/LHCC 02-26 CERN Geneva, 15 December 2002

[43] CMS Collaboration 2006 *CMS Physics Technical Design Report Vol 2* CERN/LHCC 06-021 CERN Geneva, 26 June 2006

[44] Kostyukhin V 2006 *Top quark reconstruction in ATLAS* Prepared for TOP 2006: International Workshop on Top Quark Physics, Coimbra, Portugal, 12-15 Jan 2006 PoS TOP2006:017,2006

[45] D'Hondt J, Heyninck J and Lowette S 2006 *Measurement of the cross section of single leptonic t anti-t events* CMS note CMS-NOTE-2006-064 CERN Geneva, 16 May 2006

[46] Bentvelsen S 2004 *Studies of top quark properties at the LHC* Presented at 39th Rencontres de Moriond on QCD and High-Energy Hadronic Interactions, La Thuile, Italy, 28 Mar - 4 Apr 2004 hep-ph/0408111

[47] Beneke M *et al* 2000 *Top quark physics* Talk given at Workshop on Standard Model Physics (and more) at the LHC (First Plenary Meeting), Geneva, Switzerland, 25-26 May 1999 hep-ph/0003033